Cytometry Part A 71A:327–333 (2007)

Combined Serial Section-Based 3D Reconstruction of Cervical Carcinoma Invasion Using H&E/p16^{INK4a}/CD3 Alternate Staining

Nicolas Wentzensen,[1†] Ulf-Dietrich Braumann,[2,3†*] Jens Einenkel,[4] Lars-Christian Horn,[5] Magnus von Knebel Doeberitz,[1] Markus Löffler,[6] and Jens-Peer Kuska[2]

[1]Division for Applied Tumor Biology, Institute of Pathology, University Heidelberg, 69120 Heidelberg, Germany
[2]Working Group Tissue Organization, Interdisciplinary Center for Bioinformatics, University Leipzig, 04107 Leipzig, Germany
[3]Core Unit Computational Microscopy, Translational Center for Regenerative Medicine, University Leipzig, 04103 Leipzig, Germany
[4]Department of Obstetrics and Gynecology, University Leipzig, 04103 Leipzig, Germany
[5]Working Group Gynecopathology, Institute of Pathology, University Leipzig, 04103 Leipzig, Germany
[6]Institute for Medical Informatics, Statistics and Epidemiology, University Leipzig, 04107 Leipzig, Germany

Received 7 October 2006; Accepted 28 December 2006

Background: Malignant growth and invasiveness of cancers is a function of both intratumoral and stromal factors. The accessibility to nutrients, oxygen and growth factors, the stromal composition, and the interference with the immune system all shape the tumor invasion front. A recent study has shown a prognostic difference with respect to different invasion patterns analyzed on histological specimens of cervical cancers. The present study analyzes the spatial organization of a cervical cancer and the relation of the tumor invasion front and the infiltration with CD3$^+$ T-cells.

Methods: From a cervical squamous cell carcinoma specimen, 84 serial sections were performed and three interleaving series were stained with hematoxylin/eosin and immunohistochemistry directed against the cervical carcinoma biomarker p16^{INK4a} and the T-cell marker CD3. Sections were passed through an image processing chain to obtain a reconstructed and segmented tissue volume. For local tumor invasion front analysis the mean curvature was used, which in turn was related to the respective local minimum tumor to T-cell distance as well to a T-cell originated diffusing substance's concentration at the tumor surface.

Results: Spatial models of the tumor tissue and the infiltrating T-cells were computed. The overall discrete compactness of the tumor invasion front was 0.89, corresponding to a pathological assessment of diffuse infiltration. The comparison of the tumor invasion front with the density of T-cell infiltration revealed an increased smoothening in regions with high T-cell infiltration.

Conclusions: We could demonstrate the spatial organization of a cervical cancer and model the interaction between infiltrating T-cells with the tumor invasion front shape. Increased smoothening in regions with high T-cell infiltration suggests that T-cells may have an influence on the shaping of the tumor invasion front, e.g., by attacking tumor cells displaying specific antigens. The applied technique allows visualization of the spatial organization of tissues and could be extended to analyze multiple stains on alternating sections. © 2007 International Society for Analytical Cytology

Key terms: biological tissues; tumor invasion; cervical carcinoma; T-lymphocytes; immunohistochemistry; large serial sections; image registration; image segmentation; microscopy; scientific visualization

Both cellular genotype and phenotype, as well as extratumoral factors, such as accessibility to nutrients, oxygen, and growth factors are important determinants of malignant growth and invasiveness. Thus, the tumor invasion front reflects both the malignant features of the tumor itself and the interaction between the tumor and the nondiseased surrounding tissue. Several attempts have been made to model tumor growth based on the availability of nutrients and growth factors. These approaches were able to predict the tumor shape in simple models and have shown a relationship between growth rate, nutrients and tumor shape (1). However, several other factors, such as tumor-stroma interactions based on direct cell–cell contacts and paracrine signaling have been shown to be im-

Part of this work was presented at the 11th Leipziger Workshop, April 27–29, 2006.

[†]These authors contributed equally to this work.

*Correspondence to: Ulf-Dietrich Braumann, Dr.-Ing., Translational Center for Regenerative Medicine, University Leipzig, Philipp-Rosenthal-Straße 55, 04103 Leipzig, Federal Republic of Germany.
E-mail: braumann@uni-leipzig.de

Published online 5 February 2007 in Wiley InterScience (www.interscience.wiley.com).
DOI: 10.1002/cyto.a.20385

portant determinants of tumor invasion and progression (2–4). Components of the immune system were found to modulate malignant growth. Besides many inflammatory and reactive cell types, such as macrophages, granulocytes and other innate immune cells, components of the adaptive immune system can be found infiltrating the surrounding tumors. Among them are cytotoxic T-cells that target structures expressed by tumor cells and that can attack and lyse these cells. Numerous tumor associated antigens have been identified in various tumors that were shown to elicit T-cell mediated immune responses (5). It is supposed that many malignant cells are eliminated by the immune system before detectable tumors develop. Accordingly, proliferating cancers have been shown to develop manifold immune escape strategies (6).

Cervical carcinomas are caused by persistent infections with human papilloma viruses (HPV). The deregulated expression of HPV oncogenes induces strong overexpression of the cellular $p16^{INK4a}$ protein, a biomarker that is being used to improve the histological assessment of cervical cancer (7,8). In the majority of HPV infected women, the immune system controls premalignant cells and thus prevents the development of malignant disease (9). Many cervical cancers show infiltrations with T-cells that are supposed to be directed against proteins expressed in the malignant cells. Immunological studies have demonstrated that reactive cytotoxic T-cells directed against viral proteins (E6, E7) and against over-expressed self-antigens, such as $p16^{INK4a}$ (10,11) can be isolated from cervical cancers. In addition, histological studies have been performed that have analyzed the phenotype of tumor infiltrating T-cells in detail (12). However, the spatial interaction between tumor cells and immunologic cells with possible effects on the tumor invasion pattern has not been shown previously. Recently, Horn et al. have shown that specific invasion patterns of cervical cancers have a prognostic value. In a study of over 600 cervical cancer cases, invasion patterns were assessed on microscopic slides and compared to pathologic and clinical data (13). Highly dissociative, spray-like growth was correlated with advanced tumor stages, high recurrence rates, and reduced survival. A correlation between immune infiltrations detected on hematoxylin and eosin (H&E) slides with invasion patterns was not observed. However, in this analysis, a clear differentiation of immune system components was not possible. In our present study, we used a general T-cell marker (CD3) to specifically highlight components of the adaptive immune system that might be involved in immunoediting.

In histological assessment of malignant tumors, usually only a small portion of the diseased tissue can be observed on a single slide. In many cases, serial sections have to be performed to monitor the invasiveness of a tumor over a larger area. With continuous spreading of digital (virtual) microscopy technology, the potential for the further uprating of the precision and reproducibility of morphological assessments in biomedicine is growing considerably. Linked with state-of-the-art image processing technology, at this stage automated morphometric analyses are going to be introduced in laboratory practice. Presently, a broad development towards computational microscopy can be stated. Besides the development of routine applications, image processing also offers a broad spectrum for experimental investigations regarding tissue organization. E.g., 'just' extending the well-established traditional two-dimensional (2D) microscopy by adding the third spatial dimension, three-dimensional (3D) analysis and morphometry of tumors based on conventional transmitted light microscopy using serial sections can provide important information on tumor-stroma interaction and tumor invasion. We have previously demonstrated the feasibility to generate spatial models of tumor masses and to calculate the compactness of the tumor invasion front (14). Lately, this technology could successfully be extended to both reconstruct and visualize large alternately stained histological serial sections (15). In the present study, we have analyzed this cervical squamous cell carcinoma (SCC) with triple alternative staining for H&E (reference stain, Fig. 1a), $p16^{INK4a}$ (tumor marker, Fig. 1b) and CD3 (T-lymphocyte marker, Fig. 1c) and assess the shape of tumor invasion with respect to the T-cell infiltration.

MATERIALS AND METHODS

Tissue Specimen

As primary case of investigation, we have used a specimen of a radially-cut uterine cervix obtained from a radical hysterectomy. The section plane exhibits a squamous cell carcinoma including the invasion front into the cervical stroma and was classified as follows: pT1b1, pN0, pMx, G3, L1, V0. In total, 84-serial sections were cut from the selected paraffin-embedded block (slicing thickness: 10 μm). The sections were separated into three interleaving series, each with 28 sections. Sections were immersed in xylene twice for paraffin removal and rehydrated by decreasing alcohol gradients (2 × 100%, 96%, 70% each 5 min).

Immunohistochemistry

While the first series was stained with H&E, the second series was stained with the CINtec™ $p16^{INK4a}$ histology kit (Dako GmbH, Hamburg, Germany), and the third series with an anti-CD3 antibody according to the manufacturer's prescriptions (Acris Antibodies GmbH, Hiddenhausen, Germany). In brief, $p16^{INK4a}$ staining was initiated by epitope retrieval using TRIS/EDTA pH 9.0 at 95°C for 10 min. After peroxidase blocking, the primary antibody directed against $p16^{INK4a}$ (clone E6H4) was incubated for 30 min on the slides. After washing and incubation with the visualization reagent containing the secondary antibody (anti-mouse), substrate chromogen solution containing DAB was applied for 30 min and counterstaining was performed with hematoxylin. For CD3 staining, 10 mM citrate buffer was used for epitope retrieval in the microwave oven. The primary antibody (Clone DM112) was incubated for 60 min and the secondary antibody incubation and detection reactions were performed using the Vectastain ABC Elite kit (Mouse IgG, PK-6102, Vector Laboratories, Burlingame, CA), the substrate used was on DAB chromogen (Liquid DAB, Dako GmbH, Hamburg, Germany). Counterstaining was performed with hematoxylin.

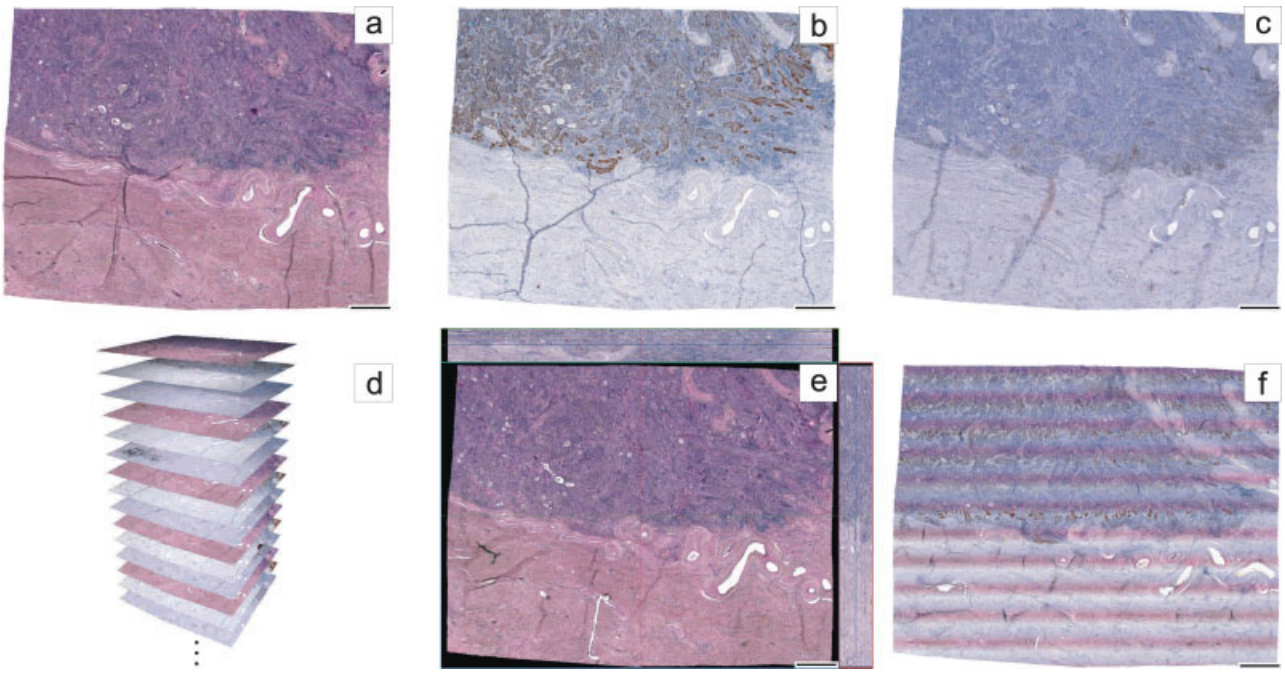

FIG. 1. Histological serial section from a uterine cervix specimen exhibiting a squamous cell carcinoma. (**a–c**) Selected triple-sequence H&E/p16^{INK4a}/CD3 (scale bar: 1 mm, the irregular outline is due to the applied registration procedures); (**d**) stack of registered alternately stained histological serial section (five triples); (**e**) multiplanar reconstruction of the complete stack (84 images); (**f**) virtual slicing plane within the 3D reconstructed tissue. The image shows a plane with 2° tilt by this passing ~33 consecutive sections. The upper half mainly consists of tumor invading into the stroma. While the tumor is more or less visible in all three staining techniques, it is best delimitable at the p16^{INK4a} slices as saturated brown structures (see (b)). Because of the high accuracy of the obtained reconstruction, while interactively browsing through the stack, tumor structures as well as vessels and many other details smoothly continue in the adjacent slices. The spatial localization of the inflammatory response between the tumor invasion front and the stroma as can be seen in the middle of the virtual plane (f) is of particular tumor-biological interest.

Microscopic Image Digitization

For all images, along the series, a corresponding region of interest (ROI) was digitized (1,300 × 1,030 pixels, area 0.865 cm^2, pixel size ~8 × 8 μm^2). This step was carried out on an Axioskop 2 plus upright brightfield transmitted light microscope equipped with an AxioCam MRc digital camera using the AxioVision 3.1 image capturing software (all products by Carl Zeiss MicroImaging GmbH, Germany). To ensure an optimum image quality, several settings were stipulated throughout all digitizations, i.e., Köhler illumination, lamp current, damping filters, and diaphragm opening. Before starting to capture, a black reference image was taken. Then, under an empty optical path the maximum exposure time was selected for an optimum adaptation to the 8 bit dynamic range. Following, the white balance correction was accomplished. An empty image was taken as reference for the shading correction, which was activated in the following. The white balance correction was then repeated.

Image Registration and 3D Reconstruction and Tissue Segmentation

Even though carefully accomplished, slicing and staining unavoidably may induce severe artifacts, mainly different kinds of distortions. To a large extent, these can be algorithmically treated using our dedicated image processing chain consisting of a series of linear and nonlinear automatic reference-free image registrations as well as an intermediate tissue segmentation step as was described in Ref. 14. Now, for the registration of images of alternately stained consecutive slices a problem arises due to a partial loss of spatial correspondences between two respective images with possibly totally different distributions both in the color as well as in the position space, unfortunately preventing the direct registration of the images. As solution we newly have introduced a consistent image segmentation step prior to the above mentioned nonlinear registration. We consider this step essential in order to obtain the optimum accuracy for the respective registration transformation. This consistent segmentation's identification of different tissue types does not only simply consider pixel color differences to build up the segmentation vector for each pixel; statistical properties within the pixel neighborhood may also be added to the vector, e.g. via sampling along an Archimedean spiral, starting at the respective pixel and analyzing the spatial frequency distribution of the one-dimensional Fourier transform. Further, the vector additionally includes color features taken from several Gaussian smoothed image instances. We basically apply a fuzzy c-means clustering method and estimate the parameters of an overall distribution (described as linear combination of normal distributions) by means of a variant of the expectation maximization algorithm (16). Using the estimated distribution we label every pixel with a class number to obtain the image segmentation, however, for a

pair of differently stained slices the segmentation results may still differ, e.g., with respect to the determined class number. This basically can occur if one of the specific staining marks certain structures which remain invisible in the corresponding slice's image. For such case the class labels have to be merged to correspondingly describe the same regions with the same labels in order to achieve the best possible consistent segmentation. Moreover, merging may also be advised if more than a single normal distribution is required to segment a certain histological structure due to staining inhomogeneities.

Once the segmentation was done for an image pair, we take the respective two scalar images to compute the displacement vector field for the nonlinear, nonparametric curvature-based registration (17). The latter requires the numerical solution of a coupled system of fourth-order partial differential equations. Finally, with the obtained displacement vector field to register one image onto its predecessor in the series, the original color image is just transformed according to this transformation in order to eventually yield—after repeated registration steps along one serial section—a reconstructed volume data set of the original image modality.

Quantitative Assessment

The reconstructed tumor volume is used to compute a polygonal approximation of the invasion surface. From the volume data the mean curvature κ can be calculated from the interpolated volume data $c(x, y, z)$. This can be accomplished as computation of the half trace of the Hessian matrix (the square matrix of second partial derivatives) of $c(x, y, z)$:

$$\kappa(x,y,z) = \frac{1}{2}\left(\frac{\partial^2 c}{\partial x^2} + \frac{\partial^2 c}{\partial y^2} + \frac{\partial^2 c}{\partial z^2}\right). \quad (1)$$

This mean curvature is computed at each center of mass $\mu_i = (x_i^*, y_i^*, z_i^*)^T$ for the set of polygons building up a polygonal approximation of the invasion surface.

To quantify the spatial relationship between the T-cells and the tumor invasion front, the pairs $(\kappa(\mu_i), d(\mu_i))$ are used, where $d(\mu_i)$ is the minimum distance from the polygon center of mass μ_i to any of the T-cells within the volume. The tumor surface has nearly half a million polygon centers and an estimate of the density distribution $p_d(\kappa, d)$ can be computed. To avoid artifacts due to the finite volume, the conditional density

$$p_d(\kappa|d) = \frac{p_d(\kappa, d)}{\int p_d(\kappa, d)d\kappa} \quad (2)$$

will be used.

To quantify the hypothesized tumor vs. T-cell relationship, and in particular to assess the T-lymphocyte infiltration strength with respect to a local tumor surface area, i.e. the influence of assumed substances produced by the T-cells that damage cancer cells, we assume that every T-cell produces and emits this substances with a constant rate t_s, and the substance with concentration c_s spreads into the volume by a diffusion process with diffusion constant D_s. Assuming zero-derivative boundary conditions for the concentration c_s, we have to solve the partial differential equation

$$-D_s \Delta c_s(x,y,z) = t_s(x,y,z) \quad (3)$$

to obtain the static concentration profile of the substance s in the volume ($\Delta = \frac{\partial^2}{\partial x^2} + \frac{\partial^2}{\partial y^2} + \frac{\partial^2}{\partial z^2}$ denotes the Laplace operator). Since, we don't know the production rate t_s and the diffusion constant D_s, we can only compute a spatial distribution that is proportional to these constants. Having the concentration profile in the volume, we can again sample the concentration on the polygon centers $(\kappa(\mu_i), c_s(\mu_i))$ and compute an estimate of the probability distribution $p_s(\kappa, c_s)$.

RESULTS

Two-Dimensional Analysis and Processing of the Tumor

The conventional H&E staining of the specimen showed a cervical squamous cell carcinoma (Fig. 1a) together with a peritumoral inflammatory response which is difficult to be differentiated on the given level of resolution (~8 μm). The complete tumor tissue showed diffuse staining pattern for $p16^{INK4a}$ (Fig. 1b). The CD3 staining showed heterogeneous T-cell clusters at the tumor invasion front (Fig. 1c). Figure 1d illustrates the stacked sections with alternating H&E, $p16^{INK4a}$, and CD3 staining for the first 15 sections. After registration of the images, a virtual oblique section with a 2° angle passing through ~33 sections was captured. Figure 1f demonstrates the high quality image processing that continuously integrates the three different stainings and allows to follow structures seamlessly through all sections (see multiplanar reconstruction in Fig. 1e).

Three-Dimensional Reconstruction of the Tumor, Analysis of Invasion Front

The reconstructed tumor appears as a sponge-like mass. The tumor invasion-front pattern exhibits a 3D discrete compactness of 0.89, which basically corresponds to the pathologist's assessment "diffuse" (cp. 14). The combined reconstructed tissue was automatically segmented with respect to the tumor ($p16^{INK4a}$, Fig. 2a) and the T-cells (CD3, Fig. 2b) and resulting segments were visualized in 3D using a polygonal approximation of the surfaces of the tumor invasion front and the T-lymphocytes, respectively. Now, the spatial relationship of the tumor invasion and the inflammatory response can be visually inspected interactively and further assessed quantitatively (Fig. 2c). Within an overall reconstructed tissue volume of 60.9 mm^3 the tumor within this volume of interest (VOI) fills 11.6 mm^3, and T-lymphocytes have been detected for another 1.1 mm^3.

Relationship Between Tumor Shape and T-Cell Infiltration

New measures both plausibly and illustratively describing the spatial relationship (colocalization) between tu-

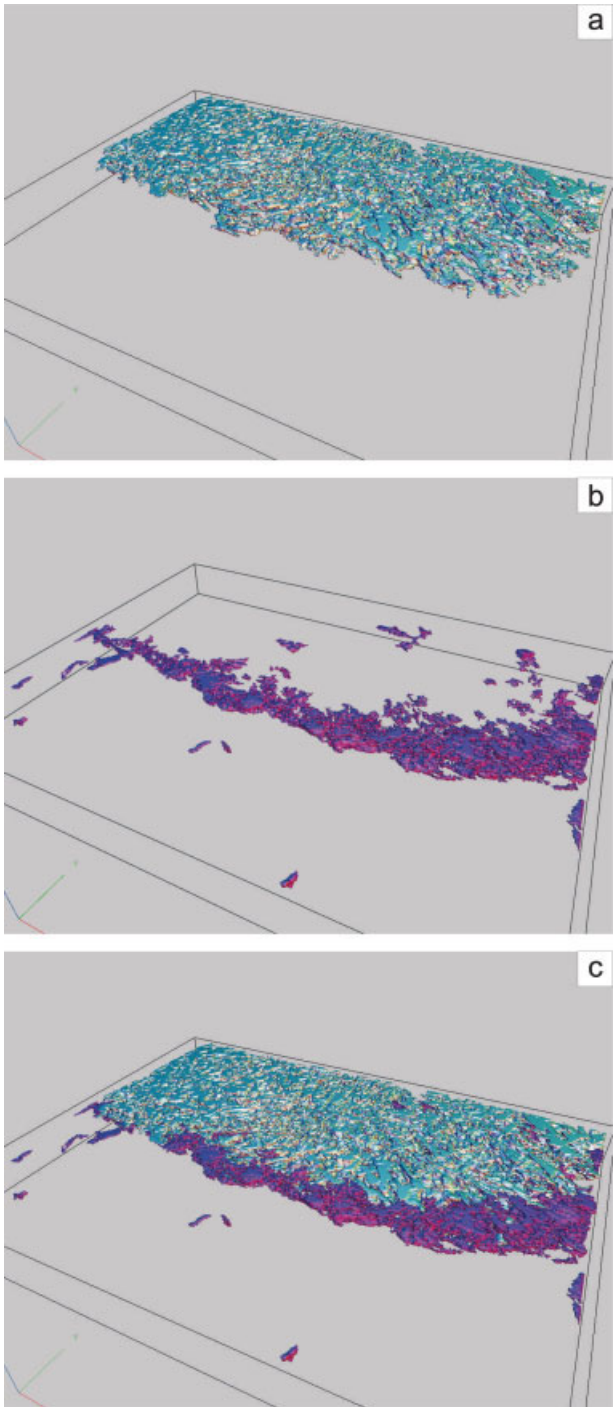

FIG. 2. In the 3D surface rendering both the automatically segmented tumor (**a**) and those tissue regions exhibiting T-lymphocytes (**b**) are shown. (**c**) Illustrates how close the T cells regions surround the tumor invasion front. The overall height of the 3D reconstructed tissue volume is 0.84 mm.

mor and T-lymphocytes have been applied. In Figure 3a, we again depict the tumor segment (as in Fig. 2a) but now apply a color code for all tumor surface polygons expressing the respective shortest distance to the T-lymphocyte segments (cp. Fig. 2b). While this mapping only allows to roughly estimate some dependence between the tumor-T-lymphocyte distance and the tumor shape, we go another step further and have identified the association between this distance and the respective shape of the tumor surface (Fig. 4) using the above introduced mean curvature [Eq. (1)]. In this plot we depict the estimated conditional probability $p_d(\kappa|d)$ [Eq. (2)]. In summary, this plot suggests that the longer the distance, the more surface regions with a high magnitude of curvature can occur. Roughly speaking, the region with a relatively high probability can be delineated by an upright "V" shape in the diagram. This also means, in regions with T-cells close to the tumor invasion front, a smoothening of the cancer surface was observed. In tumor surface regions more distant from T-cells, larger curvature values occur more frequently.

In Figure 3b we illustrate how the T-lymphocytes may penetrate the tumor by emitting substances by means of diffusion precisely under the colocalizational conditions we have found (cp. Fig. 2c). This was done by solving the

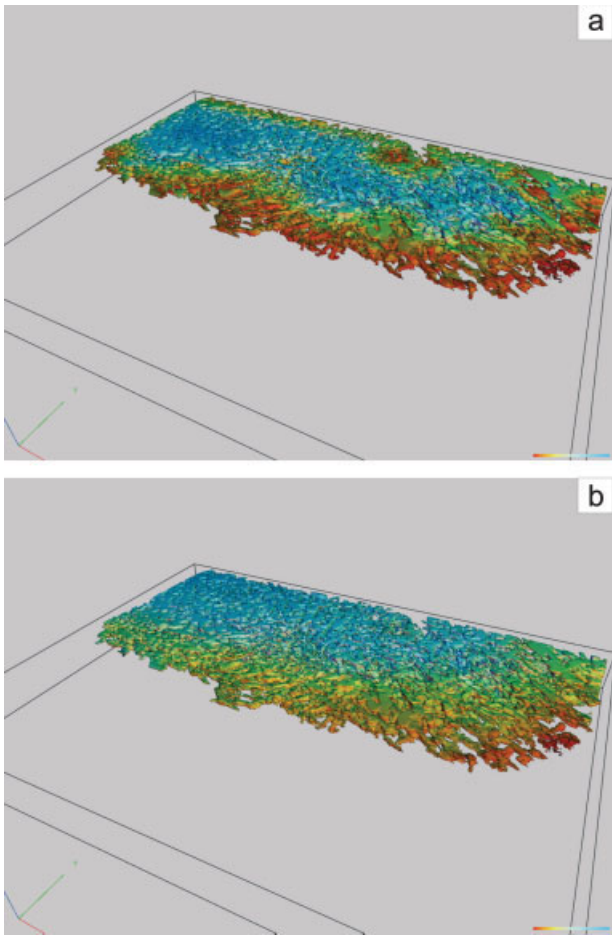

FIG. 3. Tumor-related colocalizational analysis of the neighboring T-lymphocytes. (**a**) Shortest distance between tumor invasion front and T-cells (red: short, yellow: medium, and light blue: far). (**b**) Logarithm of the concentration of T-lymphocyte emitted substances diffusing towards the tumor invasion front. The color denotes the respective concentration (red: high, yellow: medium, and light blue: low) when impinging the invading tumor's surface.

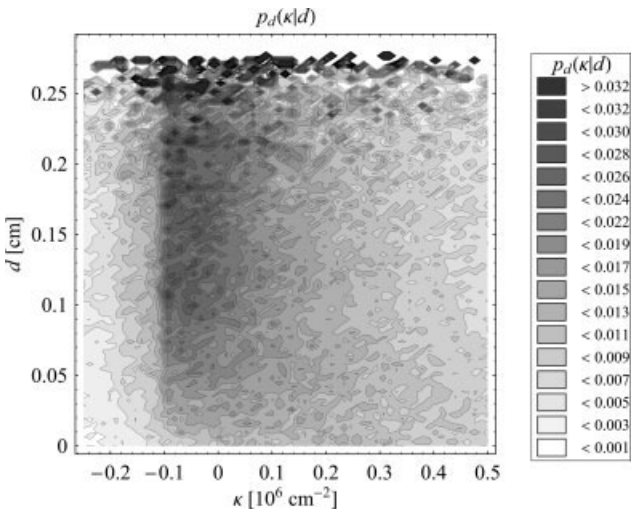

FIG. 4. Conditional probability $p_d(\kappa|d)$ for the mean curvature κ at a certain distance d from the T-cells. The longer the distance d, the more surface regions with a high magnitude of curvature κ occur. Under the influence of the T-cells a smoothening of the tumor surface (at close distances) arises, while for tumor regions more far apart from the T-cells larger curvature values occur more frequently. Negative curvatures denote convex surface areas, positive concave ones.

Eq. (3) providing us information on the local penetration strength of the diffusing molecules on the tumor surface. Therefore, every surface polygon was assigned a color indicating the logarithm of the local substance concentration. What basically can be seen roughly comparing Figure 3b with Figure 2b is that the thicker the T-lymphocyte margin appears, the higher is the concentration at the tumor surface. We therefore can assume that the concentration measure well reflects the level of T-cell invasion. Again, we would like to analyze if we see some interrelation of the colocalizational measure—T-cell emitted substance concentration in this case—and the local shape tumor shape. In Figure 5 the distribution shows that in areas with low concentrations of T-cell secreted molecules tumor surfaces with a broad range of values for the mean curvature are found, expressing a rather irregular tumor surface shape. The higher the concentration, the more this range shrinks to low absolute curvature values indicating an increasing smoothness of the shape. This kind of probability distribution which can be roughly delineated with a "V" turned upside down, shows that high concentrations lead to a smoothing of surface areas (with beforehand high absolute values for the mean curvature), while in regions with low concentrations less compact tumor structures appear.

DISCUSSION

In the current study, we have analyzed the spatial organization of a cervical carcinoma and its interaction with surrounding infiltrating T-lymphocytes by 3D reconstruction of serial sections including three interleaving staining for H&E, $p16^{INK4a}$, and CD3. The 3D reconstruction of the tumor tissue was based on the H&E staining and the $p16^{INK4a}$ staining, while the T-cell infiltration was reconstructed using the CD3 stain. The reconstruction resulted in a highly accurate spatial tumor model that allows to perform quasi-seamless virtual oblique sections through the tumor tissue. Using an interactive software, the tumor can be viewed from all angles, substructures can be highlighted and interactions can be viewed.

On the basis of spatial reconstruction, the overall discrete compactness of the tumor surface was calculated. In addition, the distribution of the infiltration of T-cells was analyzed and compared to the tumor surface. First, the direct correlation of the distance of T-cells from the tumor surface was compared to local tumor surface properties expressed by the mean curvature, a measure which can be interpreted as related to a surface smoothness or compactness. Second, since the distribution of T-cells varied substantially more than the distance from the invasion front, a diffusion model was used to put weight on the infiltration density of T-cells. Based on this diffusion model, a correlation was observed between a smooth tumor surface and a higher number of T-cells in the surrounding tissue.

While the majority of experimental oncologic studies are based on the examination of tumor cells or tumor tissue, it is becoming more and more clear that the tumor-stroma interaction and the immunoediting of tumors are very important determinants of malignant behavior. Schmeichel and Bissell have called for the use of models that are based on the spatial organization of tumor progression (18).

Our study shows the feasibility to perform spatial studies from primary tissues applying molecular markers. We have analyzed the infiltration of T-cells in the surrounding

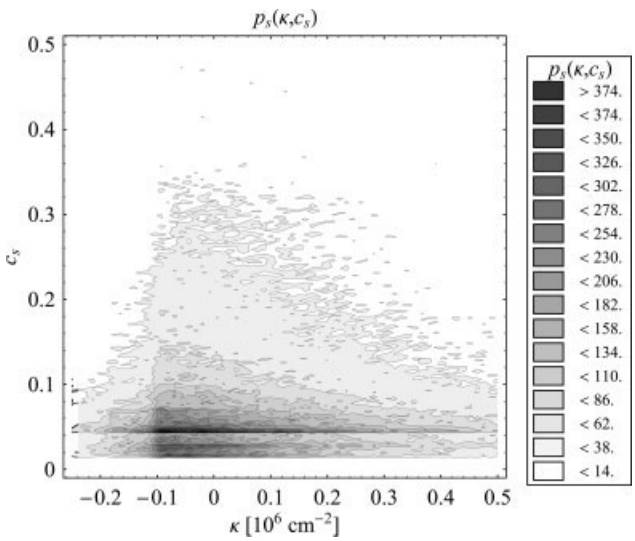

FIG. 5. Estimated probability distribution $p_s(\kappa,c_s)$ for curvature κ and substance concentration c_s emitted by the T-cells. The distribution indicates how areas with low concentrations of T-cells the surfaces of tumor invasion exhibit a broad range of values for the mean curvature, expressing a rather irregular tumor surface shape. With rising concentration, this range shrinks to low absolute curvature values. This goes along with an increasing smoothness of the tumor surface.

of a cervical cancer. The results suggest that dense T-cell infiltration altered the tumor surface to a more compact, smooth structure. The marker used for this analysis, CD3, is expressed by almost all groups of T-cells, including helper, effector and regulatory T-cells. The pure presence of $CD3^+$ cells can therefore not give any functional evidence that these cells are indeed involved in shaping of the tumor. However, the association between infiltration and tumor shape observed in our study suggests that there might be a direct relationship at least in the tumor we have analyzed.

Many other aspects of tumor growth can be analyzed using the spatial modeling approach we applied in this study. Expression of matrix metalloproteinases (MMPs) and tumor vascularization might be other interesting targets to analyze invasive growth. Since image registration is mainly based on the hematoxylin counterstain used in most IHC protocols, spatial reconstruction would be feasible using more than three interleaving stains. To summarize, with our reconstruction method using large histological serial sections combined of different stainings we could demonstrate a powerful new technique for detailed 3D visualization and analysis of complex tissue intersections.

LITERATURE CITED

1. Frieboes HB, Zheng X, Sun CH, Tromberg B, Gatenby R, Cristini V. An integrated computational/experimental model of tumor invasion. Cancer Res 2006;66:1597–1604.
2. Nelson CM, Bissell MJ. Of extracellular matrix, scaffolds, and signaling: Tissue architecture regulates development, homeostasis, and cancer. Annu Rev Cell Dev Biol 2006;22:287–309.
3. Bhowmick NA, Moses HL. Tumor-stroma interactions. Curr Opin Genet Dev 2005;15:97–101.
4. Christofori G. New signals from the invasive front. Nature 2006;441: 444–450.
5. Jager D, Jager E, Knuth A. Immune responses to tumour antigens: Implications for antigen specific immunotherapy of cancer. J Clinical Pathol 2001;54:669–674.
6. Dunn GP, Old LJ, Schreiber RD. The immunobiology of cancer immunosurveillance and immunoediting. Immunity 2004;21:137–148.
7. Klaes R, Benner A, Friedrich T, Ridder R, Herrington S, Jenkins D, Kurman RJ, Schmidt D, Stoler M, von Knebel Doeberitz M. $p16^{INK4a}$ immunohistochemistry improves interobserver agreement in the diagnosis of cervical intraepithelial neoplasia. Am J Surg Pathol 2002;26:1389–1399.
8. Wentzensen N, Bergeron C, Cas F, Eschenbach D, Vinokurova S, von Knebel Doeberitz M. Evaluation of a nuclear score for $p16^{INK4a}$-stained cervical squamous cells in liquid-based cytology samples. Cancer 2005;105:461–467.
9. Stern PL. Immune control of human papillomavirus (HPV) associated anogenital disease and potential for vaccination. J Clin Virol 2005;32 (Suppl 1):S72–S81.
10. Evans EM, Man S, Evans AS, Borysiewicz LK. Infiltration of cervical cancer tissue with human papillomavirus-specific cytotoxic T-lymphocytes. Cancer Res 1997;57:2943–2950.
11. Wentzensen N, Kaufmann A, Reuschenbach M, Linnebacher M, von Knebel Doeberitz M. $p16^{INK4a}$ is a tumor autoantigen in HR-HPV induced cancers. Proc Am Assoc Cancer Res 2005;46:5140.
12. Sheu BC, Lin RH, Lien HC, Ho HN, Hsu SM, Huang SC. Predominant Th2/Tc2 polarity of tumor-infiltrating lymphocytes in human cervical cancer. J Immunol 2001;167:2972–2978.
13. Horn LC, Fischer U, Raptis G, Bilek K, Hentschel B, Richter CE, Braumann UD, Einenkel J. Pattern of invasion is of prognostic value in surgically treated cervical cancer patients. Gynecol Oncol 2006; 103:906–911.
14. Braumann UD, Kuska JP, Einenkel J, Horn LC, Löffler M, Höckel M. Three-dimensional reconstruction and quantification of cervical carcinoma invasion fronts from histological serial sections. IEEE Trans Med Imag 2005;24:1286–1307.
15. Einenkel J, Kuska JP, Horn LC, Wentzensen N, Höckel M, Braumann UD. Combined three-dimensional microscopic visualisation of tumour-invasion front of cervical carcinoma. Lancet Oncol 2006;7:698.
16. Braumann UD, Einenkel J, Horn LC, Kuska JP, Löffler M, Scherf N, Wentzensen N. Registration of histologic colour images of different staining. In: Handels H, Ehrhardt J, Horsch A, Meinzer HP, Tolxdorff T, editors. Bildverarbeitung für die Medizin 2006. Berlin, Heidelberg:-Springer; 2006. pp 231–235.
17. Braumann UD, Kuska JP. Influence of the boundary conditions on the result of non-linear image registration. In the DVD-Proceedings of the IEEE International Conference on Image Processing, IEEE, 2005. pp I-1129–I-1132.
18. Schmeichel KL, Bissell MJ. Modeling tissue-specific signaling and organ function in three dimensions. J Cell Sci 2003;116:2377–2388.